Journal of Alloys and Compounds 505 (2010) 657–660

Contents lists available at ScienceDirect

Journal of Alloys and Compounds

journal homepage: www.elsevier.com/locate/jallcom

Microstructure and electrical characteristics of MnTa-doped ZnO–V_2O_5-ceramics with sintering

C.-W. Nahm*

Semiconductor Ceramics Lab., Department of Electrical Engineering, Dongeui University, Busan 614-714, Republic of Korea

ARTICLE INFO

Article history:
Received 3 April 2010
Received in revised form 14 June 2010
Accepted 16 June 2010
Available online 25 June 2010

Keywords:
Ceramics
Sintering
Electrical properties
Grain boundaries
Varistors

ABSTRACT

The microstructure and electrical properties of MnTa-doped ZnO–V_2O_5-ceramics with sintering was investigated. The microstructure consisted of a primary phase of ZnO grains and minor secondary phases such as $Zn_3(VO_4)_2$, ZnV_2O_4, and $TaVO_5$, which act as liquid-phase sintering aids. The sintered density decreased from 5.69 g cm^{-3} to 5.52 g cm^{-3} due to the volatility of V_2O_5 in accordance with increasing sintering temperature. The maximum nonlinear coefficient (28) was obtained at 925 °C. The donor concentration increased from 1.07×10^{18} cm^{-3} to 3.56×10^{18} cm^{-3} in accordance with increasing sintering temperature and the barrier height exhibited the maximum value (1.25 eV) at 950 °C.

1. Introduction

Zinc oxide (ZnO) is non-stoichiometric materials possessing excessive Zn ion and thus it is n-type oxide semiconductor [1]. A pure zinc oxide ceramics exhibits linear properties even at any sintering condition, whereas the zinc oxide doped with specified impurity may exhibit nonlinear properties, which give rise to the decrease of impedance in accordance with increasing voltage, so called voltage-dependent resistor (VDR) [2,4]. The structure of the VDR consists of a matrix of conductive zinc oxide grains separated by grain boundaries, which provide *p–n* junction semiconductor characteristics. The basic conduction mechanism of the VDR results from semiconductor junctions at the grain boundaries of zinc oxide grains. The VDR is a multi-junction device with a number of grains acting as a series-parallel combination between the electrical terminals. This nonlinerity of voltage–current properties is due to the presence of a double Schottky barrier (DSB) formed at active grain boundaries containing many trap states [4,5]. Owing to highly nonlinear properties, the VDR has been extensively used in the field of circuit overvoltage protection, with application ranging from a few volts in electronic circuits to millions of volts in electric power systems [6,7]. In the light of research results up to now, VDR cannot exhibit a nonlinear behavior without adding the heavy elements with large ionic radii such as Bi, Pr, etc. [2,3]. Commercial Bi_2O_3- and Pr_6O_{11}-based VDR cannot be co-fired with a silver inner-electrode (m.p. 961 °C) in a multilayered chip component because of their high sintering temperature above 1000 °C [2,3]. Therefore, the new VDR requires further research in order to use a silver inner-electrode. Of the various possible ceramics, one candidate is the ZnO–V_2O_5-based ceramics [8]. These ceramics can be sintered at a relatively low temperature of approximately 900 °C. This is important for multilayer chip component applications, because it can be co-sintered with a silver inner-electrode without using expensive Pd or Pt. The binary ZnO–V_2O_5-ceramics exhibit low nonlinear properties with a nonlinear coefficient below 10 [11–13]. In order to develop high performance nonlinear ceramics, a ZnO–V_2O_5-based ceramics containing a third additive has been actively studied [11–16]. The ternary ZnO–V_2O_5–MnO_2 (or Mn_3O_4) ceramics were revealed to possess improved nonlinear properties with a nonlinear coefficient of 17–19 [11,12]. A study of ZnO–V_2O_5-based ceramics is only initial step for application.

To improve nonlinear properties of ZnO–V_2O_5-based ceramics, it is very important to comprehend the effects of sintering process on electrical properties for the varistor ceramics with specified composition.

In this study, the microstructure and electrical properties of MnTa-doped ZnO–V_2O_5-ceramics with sintering were investigated and some new results were obtained.

2. Experimental procedure

Reagent-grade raw materials were prepared in the proportions of quaternary composition expression, such as 97.45 mol% ZnO, 0.5 mol% V_2O_5, 2.0 mol% MnO_2, and 0.05 mol% Ta_2O_5. Raw materials were mixed by ball milling with zirconia balls and acetone in a polypropylene bottle for 24 h. The mixture was dried at 120 °C for 12 h. The dried mixture mixed into container with acetone and 0.8 wt% polyvinyl

* Tel.: +82 51 890 1669; fax: +82 51 890 1664.
E-mail address: cwnahm@deu.ac.kr.

0925-8388/$ – see front matter © 2010 Elsevier B.V. All rights reserved.
doi:10.1016/j.jallcom.2010.06.102

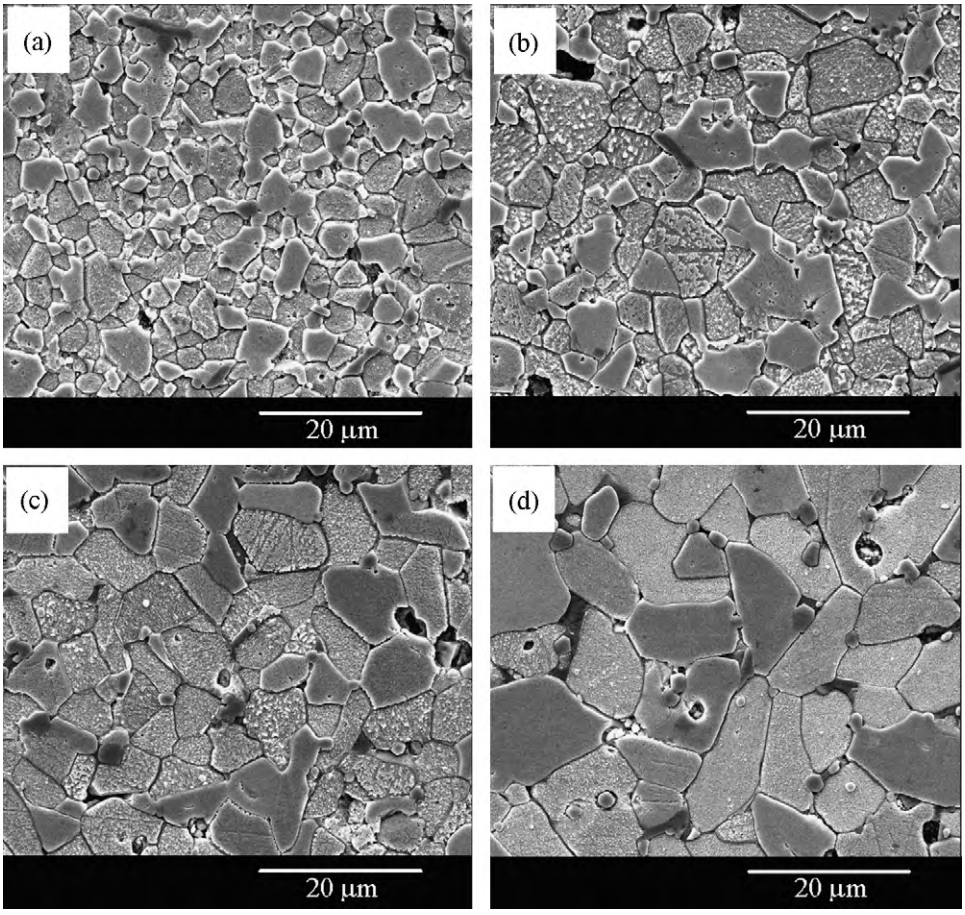

Fig. 1. SEM micrographs of the samples for different sintering temperatures: (a) 875 °C, (b) 900 °C, (c) 925 °C, and (d) 950 °C.

butyral (PVB) binder of powder weight. After drying, the mixture was granulated by sieving 100-mesh screen to produce starting powder. The powder was uniaxially pressed into discs of 10 mm in diameter and 1.5 mm in thickness at a pressure of 100 MPa. The discs were covered with raw powder in alumina crucible, sintered at four fixed sintering temperatures (875 °C, 900 °C, 925 °C, and 950 °C) in air for 3 h, and furnace-cooled to room temperature. The final samples were about 8 mm in diameter and 1.0 mm in thickness. Silver paste was coated on both faces of the samples and the ohmic contacts were formed by heating at 550 °C for 10 min. The electrodes were 5 mm in diameter.

The microstructure was examined by a field emission scanning electron microscope (FESEM, Quanta 200, Czech). The average grain size (d) was determined by the linear intercept method [17]. The crystalline phases were identified by X-ray diffractometry (XRD, X'pert-PRO MPD, Netherland) with CuKα radiation. The sintered density (ρ) of the ceramics was measured by the Archimedes method.

The breakdown field (E_B) was measured at a current density of 1.0 mA cm^{-2} and the leakage current density (J_L) was measured at 0.80E_B. In addition, the non-ohmic coefficient (α) was determined from $\alpha = 1/(\log E_2 - \log E_1)$, where E_1 and E_2 are the electric fields corresponding to 1.0 mA cm^{-2} and 10 mA cm^{-2}, respectively.

The capacitance–voltage (C–V) characteristics of the samples were measured at 1 kHz using an RLC meter (QuadTech 7600, USA) and an electrometer (Keithley 617, USA). The donor density (N_d) and the barrier height (ϕ_b) were determined by the equation $(1/C_b - 1/2C_{bo})^2 = 2(\Phi_b + V_{gb})/q\varepsilon N_d$ [18], where C_b is the capacitance per unit area of a grain boundary, C_{bo} is the value of C_b when $V_{gb} = 0$, V_{gb} is the applied voltage per grain boundary, q is the electronic charge, ε is the permittivity of ZnO ($\varepsilon = 8.5\varepsilon_o$). The density of interface states (N_t) at the grain boundary was determined by the equation: $N_t = (2\varepsilon N_d \Phi_b/q)^{1/2}$ [18] and the depletion layer width (t) of the either side at the grain boundaries was determined by the equation: $N_d t = N_t$ [19].

The dielectric characteristics, such as the apparent dielectric constant (ε_{APP}') and dissipation factor ($\tan\delta$) were measured in the range of 100 Hz to 2 MHz using an RLC meter (QuadTech 7600).

3. Results and discussion

Fig. 1 shows the SEM micrographs of the samples for different sintering temperatures. It can be easily seen that the grain structure is very homogeneously distributed and the grain boundaries are clear throughout all the ceramics, compared with existing reported literature [8–16]. The average grain size of the samples increased from 4.6 μm to 9.9 μm with the increase of sintering temperature. ZnO grains could probably grow rapidly in the presence of a rich liquid phases related to V_2O_5 because the melting point of V_2O_5 is 690 °C. The sintered density of the samples decreased from 5.69 g cm^{-3} to 5.52 g cm^{-3} corresponding to 96.5–94.5% of the theoretical density (TD) (pure ZnO, TD = 5.78 g cm^{-3}) with the increase of sintering temperature. It is assumed that the decrease of sintered density is attributed to the volatility of the V-species for V_2O_5 with low melting point. This was similar phenomenon to ZnO–V_2O_5–MnO_2 ceramics.

The XRD patterns of the samples for different sintering temperatures are shown in Fig. 2. These patterns revealed the presence of $Zn_3(VO_4)_2$, ZnV_2O_4, and $TaVO_5$ as minor secondary phases, which act as liquid-phase sintering aids, in addition to a major phase of hexagonal ZnO [8,16]. The detailed microstructure parameters are summarized in Table 1.

Fig. 3 shows the electric field–current density (E–J) characteristics of the samples for different sintering temperatures. The nonlinear properties are characterized by non-ohmicity in the E–J characteristics. The curves show the conduction characteristics divide into two regions: an ohmic region exhibiting very high impedance before breakdown field and a non-ohmic region exhibiting very low impedance after breakdown field. The sharper the knee of the curves between the two regions, the better the nonlinear properties. It can be seen from curve shapes that the sintering temperature has a significant effect on the nonlinear properties. The E–J parameters obtained from Fig. 3 are summarized in Table 1.

Table 1
Microstructure, *V–I*, *C–V*, and dielectric characteristic parameters of the samples for different sintering temperatures.

Sintering temp. (°C)	d (μm)	ρ (g cm^{-3})	E_B (V cm^{-1})	v_b (V gb^{-1})	α	J_L (mA cm^{-2})	N_d (10^{18} cm^{-3})	Φ_b (eV)	N_t (10^{12} cm^{-2})	t (nm)	$\varepsilon_{APP'}$ (1 kHz)	tan δ (1 kHz)
875	4.6	5.58	5302	2.4	8	0.5	1.07	0.56	2.38	22.2	595	0.414
900	6.4	5.54	3864	2.5	13	0.4	1.57	0.71	3.23	20.6	938	0.375
925	7.5	5.52	2715	2.0	20	0.4	2.42	0.95	4.64	19.2	1315	0.336
950	9.9	5.46	1135	1.1	28	0.1	3.56	1.25	6.12	17.2	2281	0.281

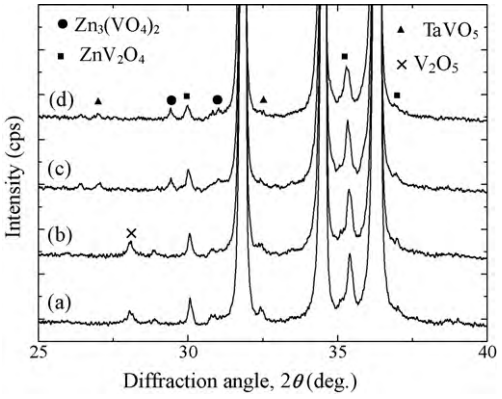

Fig. 2. XRD patterns of the samples for different sintering temperatures: (a) 875 °C, (b) 900 °C, (c) 925 °C, and (d) 950 °C.

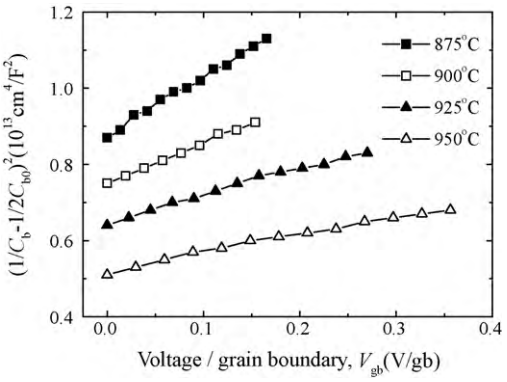

Fig. 4. *C–V* characteristics of the samples for different sintering temperatures.

The breakdown field (E_B) linearly decreased from 5302 V cm^{-1} to 1135 V cm^{-1} with the increase of sintering temperature. The behavior of E_B in accordance with sintering temperatures can be explained by the following expression: $E_B = v_b/d$, where d is the grain size and v_b is the breakdown voltage per grain boundaries. This expression indicated that the d and v_b values directly determine E_B. Therefore, the decrease of E_B in accordance with increasing sintering temperature is attributed to the increase of the average ZnO grain size and the decrease of breakdown voltage per grain boundaries. The nonlinear coefficient (α) also linearly increased from 8 to 28. It can be seen that the sintering temperature has a significant effect on the nonlinear properties in the light of the α variation. The behavior of α with sintering temperature can be related to the variation of the Schottky barrier height according to the variation of the electronic states at the grain boundaries. The sintering temperature will vary the density of the interface states with the transport of the defect ions toward the grain boundary and will be more active grain boundaries. Therefore, the increase of α in accordance with increasing sintering temperature is attributed to the increase of potential barrier height at the grain boundaries. The current density (J_L) decreased from 0.5 mA cm^{-2} to 0.1 mA cm^{-2} with the increase of sintering temperature. The J_L variation with sintering temperature was opposite to the tendency of α variation. The detailed microstructure parameters are summarized in Table 1.

Fig. 4 shows the capacitance–voltage characteristics of the samples for different sintering temperatures. The detailed *C–V* characteristic parameters, such as donor concentration (N_d) and barrier height (Φ_b), are summarized in Table 1. The N_d increased

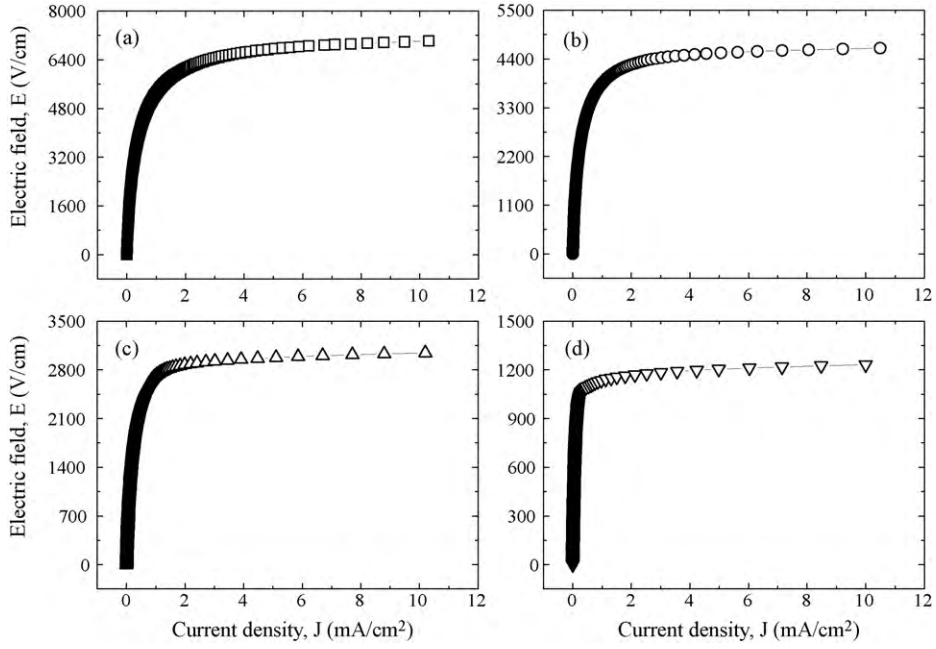

Fig. 3. *E–J* characteristics of the samples m for different sintering temperatures: (a) 875 °C, (b) 900 °C, (c) 925 °C, and (d) 950 °C.

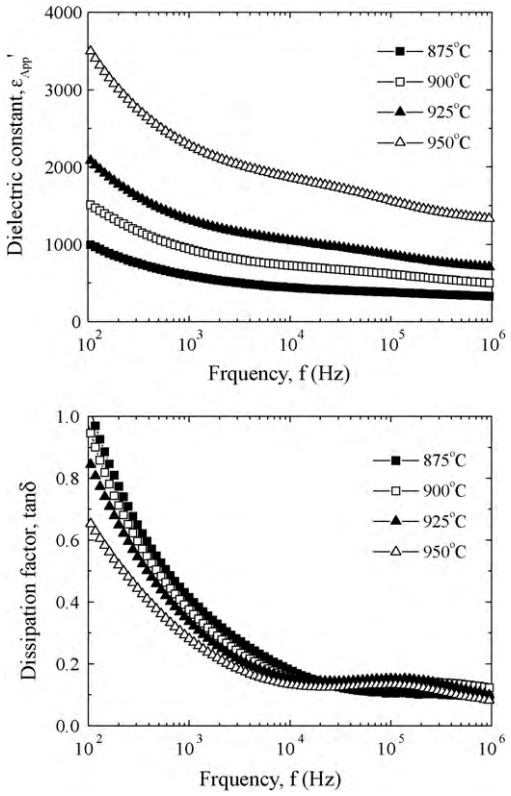

Fig. 5. Dielectric characteristics of the samples for different sintering temperatures.

from $1.07 \times 10^{18}\,cm^{-3}$ to $3.56 \times 10^{18}\,cm^{-3}$ in accordance with increasing sintering temperatures. The increase of N_d value is assumed to be due to the dissociation of zinc oxide in the following chemical reaction expression, $ZnO \rightarrow Zn_i^x + 1/2O_2$, $Zn_i^x \rightarrow Zn_i + e'$, where Zn_i^x is a neutral zinc of interstitial site, Zn_i is a positively charged zinc ion of interstitial site. It is assumed that the enhancement of the donor density results from a lot of dissociation quantities of zinc oxide when the sintering temperature increases [20]. The barrier height (Φ_b) at the grain boundaries increased in the range of 0.56–1.56 eV in accordance with increasing sintering temperatures because of a increase in density of the interface states (N_t) at the grain boundaries. This coincides with the variation of α in the *E–J* characteristics. Really, the higher barrier gives rise to the higher nonlinear coefficient. The depletion layer width (t) on either side of depletion region between grains exhibited the dependence of donor density with sintering temperatures.

Fig. 5 shows the apparent dielectric constant (ε_{APP}') and dissipation factor ($\tan\delta$) of the samples for different sintering temperatures. With increasing frequency for all samples, the ε_{APP}' abruptly decreased up to 1 kHz and thereafter it decreased gradually with less sharp dispersive drop which is closely associated with the polarization of dielectrics. The decrease rate of ε_{APP}' with frequency was found to increase in accordance with increasing sintering temperature. It is assumed that the decrease of ε_{APP}' in accordance with increasing frequency is attributed to the decrease of the number of dipole, which can follow to test frequency. The ε_{APP}' increased in the range of overall frequency in accordance with increasing sintering temperature. This is directly related to the average grain size and depletion layer width, as can be seen in the following equation, $\varepsilon_{APP}' = \varepsilon_g(d/t)$, where ε_g is the dielectric constant of ZnO (8.5), d is the average grain size, and t is the depletion layer width of the both sides at the grain boundaries. The ε_{APP}' is expected to increase because the d increases in accordance with increasing sintering temperature. The ε_{APP}' at 1 kHz increased from 592 to 2281 in accordance with increasing sintering temperature. On the other hand, the $\tan\delta$ decreased until the vicinity of 10 kHz in accordance with increasing frequency and it exhibits $\tan\delta$ peak in the vicinity of 200 kHz, and thereafter again decreased. The $\tan\delta$ at 1 kHz value increased from 0.414 to 0.282 in accordance with increasing sintering temperature. The detailed dielectric characteristic parameters are summarized in Table 1.

4. Conclusions

The microstructure and electrical properties of MnTa-doped $ZnO–V_2O_5$-ceramics with sintering were investigated. The microstructure consisted of a primary phase of ZnO grains and minor secondary phases such as $Zn_3(VO_4)_2$, ZnV_2O_4, and $TaVO_5$, which act as liquid-phase sintering aids. The sintered density decreased from $5.69\,g\,cm^{-3}$ to $5.52\,g\,cm^{-3}$ due to the volatility of V_2O_5 in accordance with increasing sintering temperature. The maximum nonlinear coefficient (28) was obtained at 950 °C. The donor concentration increased from $1.07 \times 10^{18}\,cm^{-3}$ to $3.56 \times 10^{18}\,cm^{-3}$ in accordance with increasing sintering temperature and the barrier height exhibited the maximum value (1.25 eV) at 950 °C. Increasing sintering temperature caused the increase of dielectric constant and the decrease dissipation factor.

References

[1] G.D. Mahan, J. Appl. Phys. 54 (1983) 3825.
[2] M. Matsuoka, Jpn. J. Appl. Phys. 10 (1971) 736.
[3] K. Mukae, K. Tsuda, I. Nagasawa, Jpn. J. Appl. Phys. 16 (1977) 1361.
[4] H.R. Pilipp, L.M. Levinson, J. Appl. Phys. 46 (1976) 1332.
[5] D.R. Clarke, J. Am. Ceram. Soc. 82 (1999) 485.
[6] L.M. Levinson, H.R. Philipp, Am. Ceram. Soc. Bull. 65 (1986) 639.
[7] T.K. Gupta, J. Am. Ceram. Soc. 73 (1990) 1817.
[8] J.-K. Tsai, T.-B. Wu, J. Appl. Phys. 76 (1994) 4817.
[9] J.-K. Tsai, T.-B. Wu, Mater. Lett. 26 (1996) 199.
[10] C.T. Kuo, C.S. Chen, I.-N. Lin, J. Am. Ceram. Soc. 81 (1998) 2942.
[11] H.-H. Hng, K.M. Knowles, J. Eur. Ceram. Soc. 19 (1999) 721.
[12] H.-H. Hng, K.M. Knowles, J. Am. Ceram. Soc. 83 (2000) 2455.
[13] H.-H. Hng, P.L. Chan, Mater. Chem. Phys. 75 (2002) 61.
[14] H.-H. Hng, L. Halim, Mater. Lett. 57 (2003) 1411.
[15] C.-W. Nahm, J. Mater. Sci. 42 (2007) 8370.
[16] C.-W. Nahm, Ceram. Int. 35 (2009) 2679.
[17] J.C. Wurst, J.A. Nelson, J. Am. Ceram. Soc. 55 (1972) 109.
[18] M. Mukae, K. Tsuda, I. Nagasawa, J. Appl. Phys. 50 (1979) 4475.
[19] L. Hozer, Semiconductor Ceramics: Grain Boundary Effects, Ellis Horwood, 1994, p22.
[20] M.F. Yan, A.H. Heuer, Additives and Interfaces in Electronic Ceramics, Am. Ceram. Soc. Columbus, OH, 1983, 80.